High-Q Plasmonic Crystal Laser for Ultra-Sensitive Biomolecule Detection

Jiacheng Sun, Tao Wang, Zeinab Jafari, Fei Gao, Xiao Lin, Hongsheng Chen, Gaofeng Wang, and Israel De Leon

***Abstract*—Plasmonic lasers provide a paradigm-changing approach for the generation of coherent light at the nanoscale. In addition to the usual properties of coherent radiation, the emission of plasmonic lasers can feature high sensitivity to the surrounding environment, which makes this technology attractive for developing high-performance and highly-integrated sensing devices. Here, we investigate a plasmonic laser architecture based on a high-Q plasmonic crystal consisting of a periodic arrangement of nanoholes on a thin gold film cladded with an organic-dye-doped glass layer as the gain material. We report an extensive full-wave numerical analysis of the device's lasing performance and its application as a biochemical sensor, showing that the proposed design features excellent figures of merit for surface sensing that in principle can be over an order of magnitude larger than those of previously reported high-performance plasmonic biosensor architectures.**

***Index Terms*—Active sensor, biomolecule detection, bulk sensing, photonic crystal, plamonic laser, surface sensing.**

Manuscript received September 30, 2020; revised January 7, 2021; accepted January 8, 2021. The work of Tao Wang was supported in part by the National Natural Science Foundation of China under Grant 61804036 and in part by Zhejiang Province Commonweal Project under Grant LGJ20A040001. The work of Zeinab Jafari and Israel De Leon was supported in part by CONACyT under Grant CN-17-109 and in part by the Federico Baur Endowed Chair in Nanotechnology. The work of Fei Gao was supported in part by National Natural Science Foundation of China under Grant 61801426 and in part by Zhejiang Provincial Natural Science Foundation (Z20F010018). The work of Gaofeng Wang was supported in part by National Key R&D Program Grant under Grant 2018YFE0120000 and in part by Zhejiang Provincial Key Research and Development Project Grant under Grant 2019C04003. *(Corresponding author: Tao Wang; Israel De Leon.)*

Jiacheng Sun is with the Engineering Research Center of Smart Microsensors and Microsystems of MOE, Hangzhou Dianzi University, and also with the School of Zhuoyue Honors, Hangzhou Dianzi University, Hangzhou 310018, China (e-mail: 17061423@hdu.edu.cn).

Tao Wang and Gaofeng Wang are with the Engineering Research Center of Smart Microsensors and Microsystems of MOE, Hangzhou Dianzi University, and also with the School of Electronics and Information, Hangzhou Dianzi University, Hangzhou 310018, China (e-mail: wangtao@hdu.edu.cn; gaofeng@hdu.edu.cn).

Zeinab Jafari and Israel De Leon are with the School of Engineering and Sciences, Tecnológico de Monterrey, Monterrey, Nuevo León 64849, Mexico (e-mail: Zjafari@tec.mx; ideleon@tec.mx).

Fei Gao, Xiao Lin, and Hongsheng Chen are with the Interdisciplinary Center for Quantum Information, College of Information Science and Electronic Engineering, Zhejiang University, Hangzhou 310027, China (e-mail: gaofeizju@zju.edu.cn; xiaolinbnwj@gmail.com; hansomchen@zju.edu.cn).

This article has supplementary material provided by the authors and color versions of one or more figures available at https://doi.org/10.1109/JSTQE.2021.3051493.

Digital Object Identifier 10.1109/JSTQE.2021.3051493

I. Introduction

SURFACE plasmons are optical surface waves formed by the coupling of an optical field to free electrons at the surface of a metal [1]. There exists two types of surface plasmon waves, i.e., surface plasmon polaritons (SPPs) and localized surface plasmons (LSPs). The former type refers to surface plasmon waves that propagate along open metallic surfaces, while the latter refers to standing waves confined to nanoscopic metallic structures. Their tight field confinement to the metal's surface [2], [3] enables these surface waves to probe minuscule fluctuations of the refractive index in the vicinity of the metal surface [4]–[6]. As such, surface plasmons have been extensively exploited for sensing applications. In particular, plasmonic biosensor technology has been widely used for biochemical applications because it offers high sensitivity, as well as capacity of real-time, label-free quantitative analysis on a broad variety of analytes, ranging from chemicals, through proteins and nucleic acids, to bacterial and viral pathogens [4], [6]–[10]. Numerous plasmonic biosensor architectures have been proposed and implemented throughout the years. Perhaps the most popular one is the surface plasmon resonance (SPR) architecture, a mature technology that makes use of the SPP supported by a thin metallic film [7]. Other more sophisticated architectures with chip-integration capacity include the use of SPPs in various waveguide configurations [11]–[14] and LSPs supported by metallic nanoparticles or nanoholes in metallic films [5], [8]. In addition, integration of plasmonic nanoparticles or nanofilms with optical fibers has also resulted in miniaturization and huge sensitivities compared to SPR architecture [15], [16]. Although a large sensitivity is appealing, the figure of merit (FOM) which is proportional to the quality factor (Q factor) of the resonance defines the ultimate sensing performance. Due to this fact, grating-like structures consisting of periodic arrays of plasmonic nanoparticles or nanoholes, typically known as plasmonic lattices or plasmonic crystals have recently attracted considerable attention as sensing platforms because they can support delocalized resonances with large Q factors and sensing FOM [17]–[20]. Indeed, the advances in plasmonic biosensor technology thus far represent a remarkable progress. Yet, improving the sensitivity and FOM of plasmonic biosensors is still of great importance as it would expand their scope of applications, for instance, achieving real-time, label-free single molecule detection, highly-integrated point of need systems, and robust clinical diagnosis [21]–[24].

Referring specifically to the sensor's transducer, the performance of all previously mentioned sensing architectures is ultimately limited by the optical losses of the system, which reduces the resonance's Q factor, thus limiting the interaction with the analyte [25] and degrading the device's FOM. Hence, a compelling approach to improve the sensing performance is to mitigate the plasmonic losses by incorporating optical gain in the system. Indeed, surface plasmon amplifiers and lasers have been demonstrated in the laboratory [26]–[28] and their prospects for applications are vast [29]. In particular, recent theoretical and experimental investigations have indicated that active plasmonic biosensing architectures can offer a significant improvement on the sensing performance [30]–[33]. While these pioneering investigations have reported an improved FOM over previously reported passive devices, more efforts are still required to demonstrate an active biosensor that satisfy key factors required for ultra-sensitive biomolecule detection, in particular the possibility of achieving a large FOM for surface sensing using a platform capable of operating at room temperature.

In this work, we investigate the sensing performance of an active plasmonic biosensor configuration based on a high-Q plasmonic crystal incorporating an organic gain medium. The structure consists of a thin gold film decorated with a two-dimensional periodic array of nanoholes and cladded with an optically-pumped Rhodamine 640-doped glass layer. The high-Q plasmonic Bloch mode supported by the passive structure favors plasmonic lasing with gain levels similar to those previously demonstrated in organic media at room temperature [34], [35]. We characterize the optical properties and sensing performance of the proposed structure through extensive finite-difference time-domain (FDTD) simulations incorporating the rate equations governing the time-domain dynamics of the gain medium's atomic populations. Our analysis indicates that lasing with a narrow linewidth of 0.24 nm is possible under practical conditions. Using wavelength interrogation, we show that such a narrow linewidth together with a large sensitivity result in FOM for bulk sensing as large as $\sim$1000 RIU^{-1} and a FOM for surface sensing of $\sim$65 RIU^{-1} for thin biolayers of the order of 5 nm. The bulk FOM, in this work, is superior to those experimentally reported in previous passive and active works based on wavelength interrogation [8], [31], [36], and comparable to values predicted recently for plasmonic-laser-based systems [32], [33]. The surface FOM is also at least one order of magnitude larger than that of passive plasmonic biosensors [37], [38], indicating that this sensing architecture has potential for ultra-sensitive biomolecule detection.

II. Principle of Operation and Structure Analysis

The optical properties of passive plasmonic crystals consisting of thin metallic films patterned with a two-dimensional array of holes have been studied extensively in the past both from the fundamental point of view [18], [39] and for biosensor applications [20], [40], [41]. In this section, we describe both the passive and active optical properties of the proposed plasmonic crystal structure.

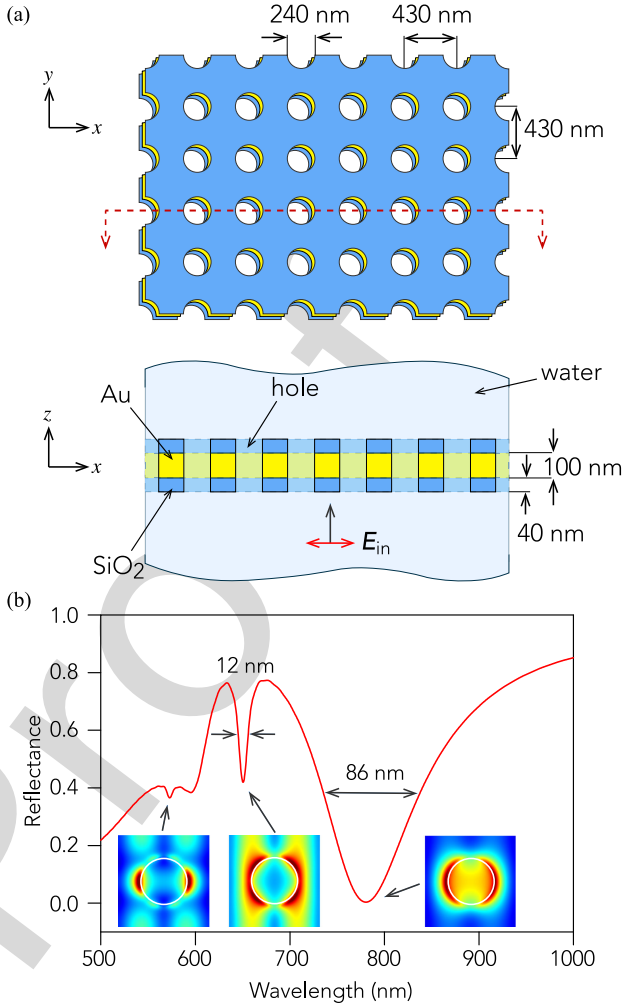

Fig. 1. Optical response of the passive structure: (a) Schematic illustration of the passive plasmonic crystal; the top panel shows a top view [(x, y)-plane] and the bottom panel shows a side view [(x, z)-plane] which is a cut along the red dashed line shown in the top panel. The medium surrounding the structure and filling the holes is water. (b) Reflection spectrum for visible and near infra-red wavelength. The broad dip corresponds to the LSP resonance of the individual nanohole, while the other two narrow dips (at 648 nm and 575 nm) are plasmonic Bloch modes of the structure. The insets illustrate the field intensity associated with the indicated spectral dips, obtained 30 nm away from the gold surface.

1) Passive Structure: We consider first the passive structure illustrated in Fig. 1(a). It consists of a gold film cladded on both sides by a thin silicon dioxide (SiO_2) layer patterned with a two-dimensional array of circular holes arranged as a squared lattice. The medium surrounding the structure and filling the holes is water. The thicknesses of the gold and each of the SiO_2 layers are 100 nm and 40 nm, respectively, the diameter of the holes is 240 nm, and the lattice period is $a = 430$ nm. We assume that the structure is illuminated by an x-polarized planewave propagating along the $+z$ direction that impinges at normal incidence onto the structure (see bottom panel of Fig. 1(a).

The optical properties of the structure are determined to a large extent by the plasmonic Bloch modes supported by the film [39]. These modes are p-polarized and can be categorized into *symmetric* or *antisymmetric* modes depending on whether the main magnetic field component has even or odd

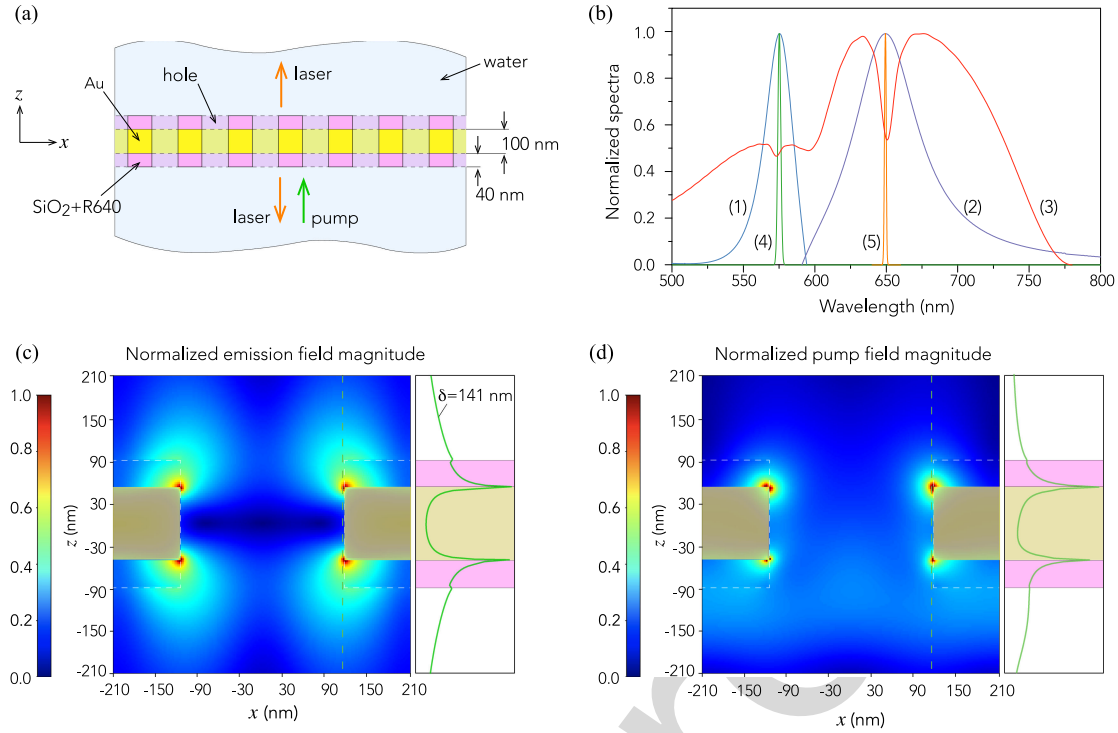

Fig. 2. Optical response of the active structure: (a) Schematic illustration of a cut through the (x, z)-plane of the active plasmonic crystal. All the parameters are the same as for the passive structure, except that the cladding is substituted by SiO_2 doped with R640 dye. (b) Relevant spectra for the active case: absorption (1) and emission (2) spectra of the R640 dye; reflection spectrum of the passive structure (3); and pump (4) and stimulated emission (5) spectra. (c) and (d) Show the normalized electric field magnitude in the (x, z)-plane through the center of the hole for the stimulated emission and pump fields, respectively. The dashed boxes superimposed indicate the location of the gain media. The curves on the right of (c,d) represent the field distribution evaluated at the points given by the dashed lines. The field in water in (c) decays exponentially with a decay constant $\delta = 141$ nm.

symmetry with respect to the $z = 0$ plane, respectively. The in-plane wavevector of these Bloch modes can be approximated by $\mathbf{k}_{\ell,m} = \mathbf{k}_{\rm SP} + \mathbf{G}$, where $\mathbf{k}_{\rm SP}$ is the wavevector of the SPP supported by the structure in the absence of the holes and $\mathbf{G} = \ell\mathbf{g}_x + m\mathbf{g}_y$ is the reciprocal lattice vector of the crystal, with $\mathbf{g}_x = \mathbf{g}_y = 2\pi/a$ being the primitive reciprocal vectors associated with the x and y directions, and ℓ and m are integers. For normal incidence illumination, only those modes with $\mathbf{k}_{\ell,m} = 0$ can be excited due to the in-plane momentum conservation, resulting in the excitation of standing-waves formed by Bloch modes with equal wavevector magnitude but opposite directions – i.e., modes associated with the indices $[\pm\ell, \pm m]$.

With this in mind, one can identify the signature of these Bloch modes in the reflectance spectrum shown in Fig. 1(b), obtained through FDTD calculations. The broad resonance, centered at the wavelength $\lambda = 778$ nm, corresponds to the symmetric $[\ell, m] = [\pm 1, 0]$ mode, while the other two narrow features centered at 648 nm and 575 nm correspond to the antisymmetric $[\pm 1, 0]$ and $[\pm 1, \pm 1]$ modes, respectively. We note that the antisymmetric $[\pm 1, 0]$ mode features a narrow linewidth of only $\sim$12 nm (corresponding to a Q factor of $\sim$54), which results from its weak coupling to radiative modes. The symmetric mode has a much broader linewidth of $\sim$86 nm. Both, symmetric and antisymmetric modes have been studied for passive sensing applications, showing similar bulk sensitivities [20]. In our case we focus on the antisymmetric $[\pm 1, 0]$ mode because its small radiative loss facilitates lasing using an optically pumped organic dye, which is attractive for its low cost and ease of fabrication.

2) Active Structure: A side view of the active structure is shown in Fig. 2(a). In this case, we have replaced the SiO_2 claddings with SiO_2 doped with Rhodamine 640 (R640) molecules, while keeping all the other structural parameters identical as those for the passive case. To model the active structure, we used an FDTD solver incorporating a semi-classical treatment for the gain medium. The semi-classical model is based on the solution of the rate equations governing the time-domain dynamics of the molecular populations in the organic gain medium [42]. The gain medium is treated as a four-energy-level system with Lorentzian emission and absorption spectra peaking at 650 nm and 575 nm, respectively. For all our simulations we have used a molecular concentration of $N = 4.5 \times 10^{19}\ \mathrm{cm}^{-3}$, and assumed that the dipole moment of such molecules is randomly oriented in space. The molecular parameters of R640 relevant for our calculations, including the radiative lifetime (4 ns) and and non-radiative damping coefficient ($3\times10^{14}\ s^{-1}$), were estimated from values previously reported in the literature for rhodamine molecules in SiO_2 at similar molecular concentration [43]. Detailed information about the FDTD model and R640 parameters can be found in the supplementary material.

The absorption (1) and emission (2) spectra of R640 used in the FDTD simulations, as well as the reflectance spectrum of the passive plasmonic crystal (3) are illustrated in Fig. 2(b). The

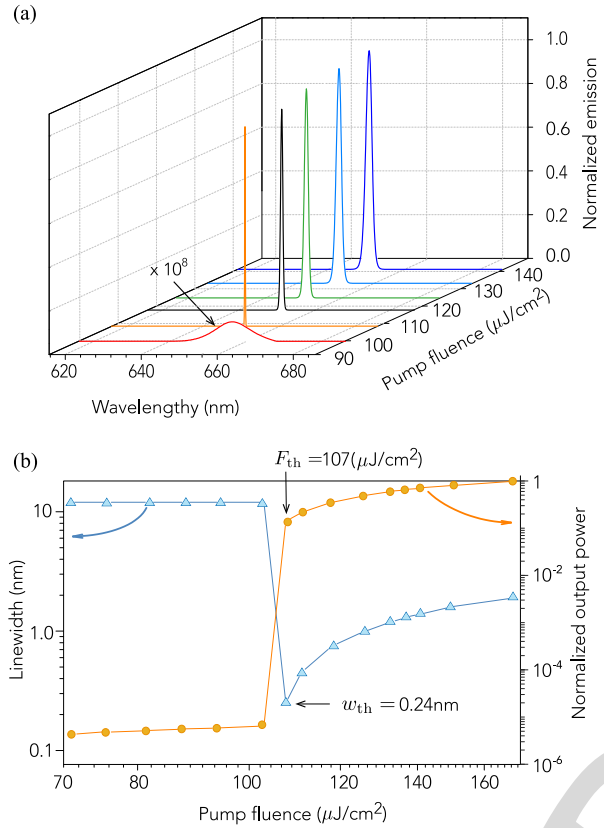

Fig. 3. Emission characteristics of the active structure: (a) Evolution of the emission spectrum as a function of the pump fluence. (b) Normalized peak value (blue circles) and spectral linewidth (orange triangles) of the emission spectrum as a function of the pump fluence. The pump threshold for laser emission is estimated as $F_{\rm th} = 107\ \mu$J/cm^2.

passive structure was optimized to support the antisymmetric $[\pm1, 0]$ and $[\pm1, \pm1]$ modes close to the peak of the emission and absorption spectra of R640, respectively, in order to facilitate the interaction of these two modes with gain medium. We have used a 200 fs pump pulse with center wavelength of $\lambda_p = 575$ nm impinging at normal incidence (see Fig. 2(a), thus exciting the $[\pm1, \pm1]$ Bloch mode of the structure. As shown in Figs. 2(c) and 2(d), this approach allows us to concentrate the pump field tightly to both surfaces of the metal film, and obtain good overlap between the pump field (the $[\pm1, \pm1]$ mode), the emission field (the $[\pm1, 0]$ mode), and the gain medium, which is crucial to achieve lasing.

The emission spectrum of the antisymmetric $[\pm1, 0]$ mode in the presence of the gain medium is calculated for a pump fluence, F, varying from 70 to 170 μJ/cm^2. The results, given in Fig. 3(a), show a broad emission spectrum characteristic of spontaneous emission for low pump fluences, and a sudden increase in the emission intensity and reduction of the spectral linewidth at $F_{\rm th} = 107\ \mu$ J/cm^2, indicating the threshold for lasing [34], [44]. The wavelength of the laser emission at the pump threshold occurs at $\lambda_e = 649.35$ nm, which is slightly shifted from the central wavelength of the antisymmetric $[\pm1, 0]$ resonance [see spectrum (1) in Fig. 2(b)]. The linewidth and normalized peak of the emission spectrum is illustrated in Fig. 3(b) as a function of F. Remarkably, the linewidth at the threshold condition is only $w_{\rm th} = 0.24$ nm and it gradually increases for larger F values. This characteristic behavior of the spectral linewidth has been reported in several experimental investigations on plasmonic nanolasers [30], [35], [44], [45]. Furthermore, similar linewidths have recently been reported experimentally for various configurations of plasmonic lasers [32], [33], [44]. The energy loss per unit length of the passive cavity can be obtained as $\alpha = \omega n_g/cQ$, where ω, c, and n_g are the angular frequency, speed of light in vacuum, and group index of the Bloch mode, respectively. Using the values $Q = 54$ and $n_g = 1.19$ obtained for the antisymmetric $[\pm1, 0]$ mode (see supplementary material), we obtain $\alpha = 2133$ cm^{-1} The threshold condition is reached when the gain supplied by the molecular medium is capable to compensate completely the loss of the cavity. However, it is important to point out that experimental investigations related to both, dielectric microlasers [46], [47] and plasmonic lasers [34], [35], have reported an enhancement in the stimulated emission rate resulting from the Purcell effect, whereby the gain provided by the molecular medium is enhanced by a factor equal to the Purcell factor of the cavity [46]. As this effect is not completely taken into account in our simulations, and our structure exhibits an averaged Purcell factor of ~ 2.1 over the gain medium (see supplementary material), we expect that the molecular concentration and pump requirements predicted by our simulations are overestimated.

III. Sensing Performance

The performance of optical biosensors are typically evaluated based on the bulk sensitivity, ($S_{\rm B}$) and surface sensitivity ($S_{\rm S}$) parameters, and their respective FOMs [8]. In particular, the $S_{\rm B}$ parameter is useful to compare the performance of different biosensor configurations, while the $S_{\rm S}$ parameter gives a more precise estimate of plasmonic affinity biosensors [48]. In what follows, we discuss the performance of the proposed active structure for both, bulk and surface sensing, assuming a constant pump fluence equal to the threshold pump fluence, $F_{\rm th}$.

We focus first on the bulk sensing performance. For spectral interrogation, the bulk sensitivity is given by $S_{\rm B} = \Delta\lambda/\Delta n_{\rm B}$, where $\Delta\lambda$ is the spectral shift of the sensing signal (the peak lasing wavelength) and $n_{\rm B}$ is the refractive index of the bulk analyte solution, which is close to the refractive index of water ($\sim$1.33). Thus, to obtain the value of $S_{\rm B}$, we assume that the refractive index of the medium around the biosensing structure is in the range $1.33 < n_{\rm B} < 1.336$. Figs. 4 a and 4(b) show FDTD calculations of the emission spectrum and peak emission wavelength as a function of $n_{\rm B}$ at the threshold pump fluence, $F_{\rm th}$. We observe a linear shift in the peak emission wavelength and no detectable change in the spectrum's linewidth. Thus, the bulk sensitivity is $S_{\rm B} = 240$ nm/RIU, obtained as the slope of the curve in Figs. 4(b), which yields a figure of merit of FOM$_{\rm B}$ = $S_{\rm B}/w_{\rm th} = 1000$ RIU^{-1} at the lasing threshold condition.

The values of $S_{\rm B}$ and FOM$_{\rm B}$ as a function of the pump fluence are shown in Fig. 4 c. Interestingly, we note that the $S_{\rm B}$ is slightly larger below the lasing threshold. This is the result of a modest reduction in the electric field's decay constant at the lasing onset [49]. Despite this fact, the FOM$_{\rm B}$ is quite

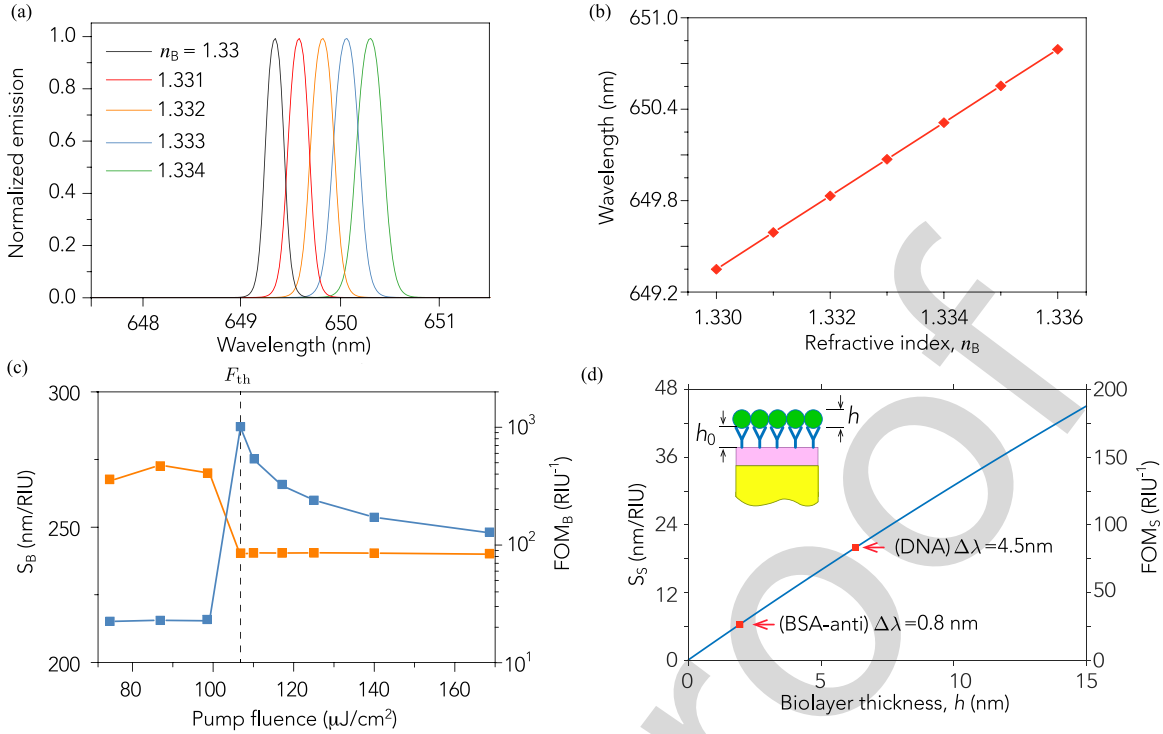

Fig. 4. Sensing performance of the active structure: (a) Spectral shift of laser emission as a function of the analyte's bulk refractive index, n_B. (b) Wavelength of emission peak as a function of n_B. (c) Bulk sensitivity (S_B, orange curve) and bulk sensing figure of merit (FOM_B, blue curve) as a function of the pump fluence. The vertical dashed line indicate the threshold condition. (d) Surface sensitivity, S_S, and surface sensing figure of merit, FOM_S, as a function of the biolayer thickness, h, for $h_0 = 2.5$ nm and $w = w_{th}$.

small below threshold due to the large spectral linewidth. On the other hand, the FOM_B peaks at the threshold condition and monotonically drops as the pump fluence increases because of the increasing spectral linewidth(see Fig. 3(b). The FOM_B value obtained at the lasing threshold is significantly larger than that of high-performance passive plasmonic biosensors [7], [8] and experimentally demonstrated room-temperature active plasmonic sensors using spectral interrogation [31], [36].

Now, we focus on the surface sensing performance. The surface sensitivity is described by $S_S = \Delta\lambda/\Delta n_S$, where n_S is the refractive index change induced by an analyte biolayer of thickness h located at a distance h_0 from the biosensor's surface. Furthermore, it is well established that this figure can be expressed as [8]

$$S_S = S_B \exp(-2h_0/\delta)\left[1 - \exp(-2\,h/\delta)\right], \qquad (1)$$

where δ is the decay constant of the field into the analyte solution. The corresponding figure of merit is therefore $FOM_S = S_S/w$. For definitiveness, we consider a value of $h_0 = 2.5$ nm corresponding to the monolayer thickness of a typical bioreceptor proteins, such as A/G protein or bovine serum albumin (BSA) [50]. The values obtained for S_S using Eq. (1) at the lasing threshold condition are shown in Fig. 4 d. For this, we have used $w = w_{th} = 0.24$ nm and $\delta = 142.8$ nm, which corresponds to the decay constant averaged over the surface of the structure (see supplementary material). Note that despite the relatively large decay constant δ, the value of S_S can be as large as 40 nm/RIU within the first 15 nm above the bioreceptor layer. From these results, we can estimate the wavelength shift induced by the analyte biolayer as $\Delta\lambda = S_S \Delta n_S$, with $\Delta n_S = 0.24$ being the refractive index difference between water and a densely packed protein biolayer [51]. Thus, considering for instance a monolayer of BSA antibody (BSA-anti), whose thickness is $h \approx 1$ nm, we obtain $\Delta\lambda \approx 0.8$ nm. Similarly, a monolayer of a larger molecule such as DNA ($h \approx 6$ nm [52]), would results in $\Delta\lambda \approx 4.5$ nm. Clearly, the predicted spectral shifts are significantly larger than the spectral linewidth, indicating the possibility of sensing minuscule changes at the surface provided that the spectral properties of the laser remain stable. The large values of $\Delta\lambda$ compared to w_{th} reflect the large FOM_S of the biosensor (right scale on Fig. 4(d), which can reach a value of 125 RIU^{-1} for biolayers with a thickness in the order of 10 nm. This is contrary to the behavior observed in a passive plasmonic biosensor [49], [53] because both, S_S and w, are inversely proportional to δ. Thus, while a small δ certainly results in a larger S_S in a passive plasmonic biosensor, it does not necessary increases its FOM_S. On the other hand, the FOM_S can be greatly increased in the active configuration because the narrow linewidth w is dictated by the pump fluence (Figs. 3(b) and 4(a) and is not influenced by the value of δ. For comparison, we have estimated the FOM_S values of typical passive plasmonic biosensors. By inserting previously reported values for plasmonic sensors, operating in a wavelength range similar to that used in this work, [38] into Eq. (1), and assuming $h = 10$ nm, FOM_S of 2.2 and 3.6 RIU^{-1} was obtained for LSPR and SPR sensors, respectively. Also, a FOM_S of 10 RIU^{-1} for $h = 10$ nm was achieved in a structure based on lattice-plasmon resonance [37]. Based on this observation we can anticipate that

the active design studied here can offer an excellent surface sensing performance.

IV. Summary and Conclusion

In conclusion, we have investigated the sensing performance of an active biosensor based on a plasmonic crystal structure incorporating an organic gain medium. The plasmonic crystal supports a high-Q Bloch mode that favors plasmonic lasing with gain levels practically attainable by organic gain media at room temperature. The optical properties, and the bulk and surface sensing performance are investigated through extensive FDTD simulations incorporating the rate equations governing the atomic population dynamics of the gain medium. Our analysis indicates that lasing with a narrow linewidth of 0.24 nm is possible under practical optical pumping conditions. We showed that the narrow laser linewidth together with a large sensitivity result in FOM for bulk sensing as large as $\sim$1000 RIU^{-1}, which is at least an order of magnitude larger than that of high-performance passive plasmonic biosensors previously reported. We also show that FOM for surface sensing can be extremely large, reaching values of $\sim$65 RIU^{-1} for thin biolayers in the order of 5 nm. We emphasize that a large surface sensing FOM is possible despite a relatively weak field confinement because, contrary to passive plasmonic sensors, the linewidth of the sensing signal is to a large extent independent of the plasmonic field confinement. The outstanding FOM values for bulk and surface sensing predicted here indicate that a high-Q active sensing architectures, such as the one studied here, have potential for low-concentration biomolecule detection.

Acknowledgment

J. Sun and T. Wang are grateful to Prof. Renmin Ma for discussion.

References

[1] S. A. Maier, *Plasmonics: Fundamentals and Applications*. New York, NY, USA: Springer, 2007.
[2] W. L. Barnes, A. Dereux, and T. W. Ebbesen, "Surface plasmon subwavelength optics," *Nature*, vol. 424, no. 6950, pp. 824–830, Aug. 2003.
[3] J. A. Schuller *et al.*, "Plasmonics for extreme light concentration and manipulation," *Nat. Mater.*, vol. 9, pp. 193–204, 2010.
[4] S. Lal, S. Link, and N. J. Halas, "Nano-optics from sensing to waveguiding," *Nat. Photon.*, vol. 1, no. 11, pp. 641–648, Nov. 2007.
[5] J. N. Anker, W. P. Hall, O. Lyandres, N. C. Shah, J. Zhao, and R. P. Van Duyne, "Biosensing with plasmonic nanosensors," *Nat. Mater.*, vol. 7, pp. 442–453, 2008.
[6] A. G. Brolo, "Plasmonics for future biosensors," *Nat. Photon.*, vol. 6, no. 11, pp. 709–713, Nov. 2012.
[7] J. Homola, Ed., *Surface Plasmon Resonance Based Sensors, Ser. Springer Ser. Chem. Sensors Biosensors*, vol. 4, Berlin, Heidelberg: Springer Berlin Heidelberg, 2006. [Onine]. Available: https://link.springer.com/book/10.1007/b100321
[8] B. pakov, P. Wrobel, M. Bockova, and J. Homola, "Optical biosensors based on plasmonic nanostructures: A review," *Proc. IEEE Proc. IRE*, vol. 104, no. 12, pp. 2380–2408, Dec. 2016.
[9] A. B. Dahlin, N. J. Wittenberg, F. Hk, and S.-H. Oh, "Promises and challenges of nanoplasmonic devices for refractometric biosensing," *Nanophotonics*, vol. 2, no. 2, pp. 83–101, 2013.
[10] J. A. Jackman, A. Rahim Ferhan, and N.-J. Cho, "Nanoplasmonic sensors for biointerfacial science," *Chem. Soc. Rev.*, vol. 46, no. 12, pp. 3615–3660, 2017.
[11] J. Dostalek *et al.*, "Surface plasmon resonance biosensor based on integrated optical waveguide," *Sensors Actuators, B: Chem.*, vol. 76, pp. 8–12, 2001.
[12] O. Krupin, H. Asiri, C. Wang, R. N. Tait, and P. Berini, "Biosensing using straight long-range surface plasmon waveguides," *Opt. Exp.*, vol. 21, no. 1, p. 698, Jan. 2013.
[13] W. R. Wong, F. R. M. Adikan, and P. Berini, "Long-range surface plasmon y-junctions for referenced biosensing," *Opt. Exp.*, vol. 23, no. 24, Nov. 2015, Art. no. 31098.
[14] Y. Gao, Q. Gan, Z. Xin, X. Cheng, and F. J. Bartoli, "Plasmonic mach-zehnder interferometer for ultrasensitive on-chip biosensing," *Amer. Chem. Soc. Nano*, vol. 5, pp. 9836–9844, 2011.
[15] H. Han *et al.*, "A large detection-range plasmonic sensor based on an h-shaped photonic crystal fiber," *Sensors*, vol. 20, no. 4, 2020, Art. no. 1009.
[16] Y. Esfahani Monfared, "Overview of recent advances in the design of plasmonic fiber-optic biosensors," *Biosensors*, vol. 10, no. 7, 2020, Art. no. 77.
[17] F. J. Garca de Abajo, "Colloquium : Light scattering by particle and hole arrays," *Rev. Modern Phys.*, vol. 79, no. 4, pp. 1267–1290, Oct. 2007.
[18] F. J. Garcia-Vidal, L. Martin-Moreno, T. W. Ebbesen, and L. Kuipers, "Light passing through subwavelength apertures," *Rev. Modern Phys.*, vol. 82, no. 1, pp. 729–787, Mar. 2010.
[19] V. G. Kravets, A. V. Kabashin, W. L. Barnes, and A. N. Grigorenko, "Plasmonic surface lattice resonances: A review of properties and applications," *Chemincal Rev.*, vol. 118, pp. 5912–5951, 2018.
[20] M. Vala, C. T. Ertsgaard, N. J. Wittenberg, and S.-H. Oh, "Plasmonic sensing on symmetric nanohole arrays supporting high-q hybrid modes and reflection geometry," *Amer. Chem. Soc. Sensors*, vol. 4, no. 12, pp. 3265–3274, Dec. 2019.
[21] P. Zijlstra, P. M. Paulo, and M. Orrit, "Optical detection of single non-absorbing molecules using the surface plasmon resonance of a gold nanorod," *Nat. Nanotechnol.*, vol. 7, pp. 379–382, 2012.
[22] S. Chen, Mikael Svedendahl, R. P. Van Duyne, and K. Mikael, "Plasmon-enhanced colorimetric elisa with single molecule sensitivity," *Nano Lett.*, vol. 11, pp. 1826–1830, 2011.
[23] J. Liu, M. Jalali, S. Mahshid, and S. Wachsmann-Hogiu, "Are plasmonic optical biosensors ready for use in point-of-need applications?*" Analyst*, vol. 45, pp. 364–384, 2020.
[24] E. Mauriz, P. Dey, and L. M. Lechuga, "Advances in nanoplasmonic biosensors for clinical applications," *Analyst*, vol. 144, pp. 7105–7129, 2019.
[25] B. Dastmalchi, P. Tassin, T. Koschny, and C. M. Soukoulis, "A new perspective on plasmonics: Confinement and propagation length of surface plasmons for different materials and geometries," *Adv. Opt. Mater.*, vol. 4, pp. 177–184, 2016.
[26] P. Berini and I. De Leon, "Surface plasmon-polariton amplifiers and lasers," *Nat. Photon.*, vol. 6, pp. 16–24, 2012.
[27] Z. Wang, X. Meng, A. V. Kildishev, A. Boltasseva, and V. M. Shalaev, "Nanolasers enabled by metallic nanoparticles: From spasers to random lasers," *Laser Photon. Rev.*, vol. 11, pp. 1–15, 2017.
[28] H. Wu *et al.*, "Plasmonic nanolasers: Pursuing extreme lasing conditions on nanoscale," *Adv. Opt. Mater.*, vol. 7, pp. 1–16, 2019.
[29] R.-M. Ma and R. F. Oulton, "Applications of nanolasers," *Nat. Nanotechnol.*, vol. 14, pp. 12–22, 2019.
[30] R.-M. Ma, S. Ota, Y. Li, S. Yang, and X. Zhang, "Explosives detection in a lasing plasmon nanocavity," *Nat. Nanotechnol.*, vol. 9, no. 8, pp. 600–604, Aug. 2014.
[31] S. Wang *et al.*, "High-yield plasmonic nanolasers with superior stability for sensing in aqueous solution," *ACS Photon.*, vol. 4, no. 6, pp. 1355–1360, Jun. 2017.
[32] W. Zhu *et al.*, "Surface plasmon polariton laser based on a metallic trench fabry-perot resonator," *Sci. Adv.*, vol. 3, no. 10, Oct. 2017, Art. no. e1700909.
[33] P.-J. Cheng *et al.*, "High-performance plasmonic nanolasers with a nanotrench defect cavity for sensing applications," *ACS Photon.*, vol. 5, no. 7, pp. 2638–2644, Jul. 2018.
[34] J. Y. Suh *et al.*, "Plasmonic bowtie nanolaser arrays," *Nano Lett.*, vol. 12, no. 11, pp. 5769–5774, Nov. 2012.
[35] A. Yang *et al.*, "Real-time tunable lasing from plasmonic nanocavity arrays," *Nat. Commun.*, vol. 6, no. 1, Nov. 2015, Art. no. 6939.
[36] X.-Y. Wang *et al.*, "Lasing enhanced surface plasmon resonance sensing," *Nanophotonics*, vol. 6, no. 2, pp. 472–478, Mar. 2017.
[37] B. pakov and J. Homola, "Sensing properties of lattice resonances of 2D metal nanoparticle arrays: An analytical model," *Opt. Exp.*, vol. 21, 2013, Art. no. 27490.

[38] B. pakov, M. L. Ermini, and J. Homola, "High-performance biosensor exploiting a light guidance in sparse arrays of metal nanoparticles," *Opt. Lett.*, vol. 44, no. 7, pp. 1568–1571, 2019.
[39] W. Dickson, G. A. Wurtz, and A. V. Zayats, Photonics: Photonics technology and instrumentation, III. Wiley, 2015, *ch. 3 - Plasmonic Crystals: Controlling Light With Periodically Structured Metal Films*, Available: https://link.springer.com/book/10.1007/b100321
[40] V. Malyarchuk *et al.*, "High performance plasmonic crystal sensor formed by soft nanoimprint lithography," *Opt. Exp.*, vol. 13, 2005, Art. no. 5669.
[41] A. De Leebeeck, K. Kumar, A. G. Brolo, R. Gordon, and D. Sinton, "On-chip detection with nanohole arrays," *Anal. Chem.*, pp. 4094–4100, 2007.
[42] S.-H. Chang and A. Taflove, "Finite-difference time-domain model of lasing action in a four-level two-electron atomic system," *Opt. Exp.*, vol. 12, 2004, Art. no. 3827.
[43] A. Lewkowicz *et al.*, "Concentration-dependent fluorescence properties of rhodamine 6 G in titanium dioxide and silicon dioxide nanolayers," *The J. Phys. Chem. C*, vol. 116, no. 22, pp. 12 304–12 311, 2012.
[44] T. K. Hakala *et al.*, "Lasing in dark and bright modes of a finite-sized plasmonic lattice," *Nat. Commun.*, vol. 8, no. 1, Apr. 2017, Art. no. 13687.
[45] H. T. Rekola, T. K. Hakala, and P. Trm, "One-dimensional plasmonic nanoparticle chain lasers," *ACS Photon.*, vol. 5, no. 5, pp. 1822–1826, May 2018.
[46] A. J. Campillo, J. D. Eversole, and H. B. Lin, "Cavity quantum electrodynamic enhancement of stimulated emission in microdroplets," *Phys. Rev. Lett.*, vol. 4, pp. 437–440, 1991.
[47] M. Djiango, T. Kobayashi, and W. J. Blau, "Cavity-enhanced stimulated emission cross section in polymer microlasers," *Appl. Phys. Lett.*, vol. 93, no. 14, Oct. 2008, Art. no. 143306.
[48] J. Li *et al.*, "Revisiting the surface sensitivity of nanoplasmonic biosensors," *Amer. Chem. Soc. Photon.*, vol. 2, pp. 425–431, 2015.
[49] F. Mazzotta *et al.*, "Influence of the evanescent field decay length on the sensitivity of plasmonic nanodisks and nanoholes," *Amer. Chem. Soc. Photon.*, vol. 2, pp. 256–262, 2015.
[50] Z. Wang, C. He, X. Gong, J. Wang, and T. Ngai, "Measuring the surface-surface interactions induced by serum proteins in a physiological environment," *Langmuir*, vol. 32, pp. 12 129–12 136, 2016.
[51] Y. Gao, Z. Xin, Q. Gan, X. Cheng, and F. J. Bartoli, "Plasmonic interferometers for label-free multiplexed sensing," *Opt. Exp.*, vol. 21, p. 5859, 2013.
[52] M. Piliarik *et al.*, "High-resolution biosensor based on localized surface plasmons," *Opt. Exp.*, vol. 20, p. 672, 2012.
[53] M. Svedendahl, S. Chen, A. Dmitriev, and M. Kll, "Refractometric sensing using propagating versus localized surface plasmons: A direct comparison," *Nano Lett.*, vol. 9, pp. 4428–4433, 2009.

Jiacheng Sun is currently studying with Hangzhou Dianzi University, Hangzhou, China. His research mainly focuses on light–matter interaction in low-dimensional structures, especially exploring novel optical properties of nanolasers.

Tao Wang received the Ph.D. degree in physics from the Université de Nice-Sophia Antipolis, Nice, France, in 2016. From 2013 to 2016, he was with the Institut Non Linéaire de Nice (now the Institut de Physique de Nice), Nice, France, as a Ph.D. Student. Since 2016, he has been a Postdoctoral Fellow with the Institut National de la Recherche Scientifique, Quebec City, QC, Canada. He is currently an Associate Professor with the School of Electronics and Information, Hangzhou Dianzi University, Hangzhou, China. His research interests include micro or nanoscale laser dynamics, optical sensors based on lasers, nonlinear optics, light–matter interactions, and optical materials.

Zeinab Jafari received the Ph.D. degree in electrical engineering from Shiraz University, Shiraz, Iran, in 2018. She is currently a Postdoctoral Fellow with Nanophotonics Research Laboratory, School of Engineering and Sciences, Tecnologico de Monterrey, Monterrey, Mexico. Her research interests include plasmonics, nanophotonics, integrated optics, and nonlinear optics.

Fei Gao received the master's degree in condensed matter physics from Nanjing University, Nanjing, China, and the Ph.D. degree in physics and applied physics from Nanyang Technological University (NTU), Singapore, in 2016. Prior to NTU, he held a research position with Biomedical Optics, the Shenzhen Institutes of Advanced Technology, Shenzhen, China. He currently holds a tenure-track position with Zhejiang University, Hangzhou, China. His current research interests include electromagnetic wave theory, topological electromagnetics, metamaterials, plasmonics, and photonic crystals.

Xiao Lin received the B.S. degree in 2011 in optical science and engineering from Zhejiang University, Hangzhou, China, where he is currently working toward the Ph.D. degree with the College of Information Science and Electronic Engineering. During the Ph.D. studies, he was a Visiting Student with the Nanyang Technological University, Singapore, and the Massachusetts Institute of Technology, Cambridge, MA, USA. His current research interests include 2-D materials, surface plasmons, and electromagnetic radiation.

Hongsheng Chen received the B.S. and Ph.D. degrees in electrical engineering from Zhejiang University, Hangzhou, China, in 2000 and 2005, respectively. In 2005, he joined as an Assistant Professor with Zhejiang University, where he was an Associate Professor in 2007 and a Full Professor in 2011. From 2006 to 2008, he was a Visiting Scientist with the Research Laboratory of Electronics, Massachusetts Institute of Technology, Cambridge, MA, USA, where he was a Visiting Professor from 2013 to 2014. His current research interests include metamaterials, invisibility cloaking, transformation optics, and theoretical and numerical methods of electromagnetics. He was the recipient of the National Excellent Doctoral Dissertation Award in China in 2008, the Zhejiang Provincial Outstanding Youth Foundation in 2008, the National Youth Top-Notch Talent Support Program in China in 2012, the New Century Excellent Talents in University of China in 2012, the National Science Foundation for Excellent Young Scholars of China in 2013, the Distinguished Chang Jiang Scholar Professorship from the Chinese Ministry of Education in 2014, and the National Science Foundation for Distinguished Young Scholars of China in 2016. He is a Regular Reviewer for many international journals on electromagnetics, physics, optics, and electrical engineering, the Topical Editor of the *Journal of Optics*, and is on the Editorial Board of Nature's *Scientific Reports* and *Progress in Electromagnetics Research*.

Gaofeng Wang received the Ph.D. degree in electrical engineering from the University of Wisconsin-Milwaukee, Milwaukee, WI, USA, in 1993, and the Ph.D. degree in scientific computing from Stanford University, Stanford, CA, USA, in 2001. From 1993 to 1996, he was a Scientist with Tanner Research, Inc., Pasadena, CA. From 1996 to 2001, he was a Principal Research and Development Engineer with Synopsys, Inc., Mountain View, CA. In 1999, he was a Consultant with Bell Laboratories, Murray Hill, NJ, USA. From 2001 to 2003, he was a Chief Technology Officer of Intpax, Inc., San Jose, CA. From 2004 to 2010, he was a Chief Technical Officer with Siargo Inc., Santa Clara, CA. From 2004 to 2013, he was a Professor and the Head with the CJ Huang Information Technology Research Institute, Wuhan University, Wuhan, China. From 2010 to 2013, he was the Chief Scientist with Lorentz Solution, Inc., Santa Clara. He is currently a Distinguished Professor with Hangzhou Dianzi University, Hangzhou, China. He has authored or coauthored more than 210 journal articles and holds 30 patents. His current research interests include integrated circuit and microelectromechanical system design and simulation, computational electromagnetics, electronic design automation, and wavelet applications in engineering.

Israel De Leon received the Ph.D. degree in electrical engineering from the University of Ottawa, Ottawa, ON, Canada, in 2011 for his theoretical and experimental work in active plasmonics. His Ph.D. dissertation was recognized with the Governor General's Gold Medal for the highest academic standing at the graduate level in Canada. He was a Postdoctoral Fellow and a Research Associate with the Max Planck Centre for Extreme and Quantum Photonics, Canada. Since 2018, he has been a Faculty Member and Leader of the Nanophotonics Research Laboratory at the School of Engineering and Sciences, Tecnologico de Monterrey, Monterrey, Mexico. Since 2019, he has also been an Adjoint Professor with the School of Engineering and Computer Sciences, University of Ottawa. His research interest include, both theoretical and experimental, plasmonics, nanophotonics, and nonlinear optics, aiming at multidisciplinary applications.

High-Q Plasmonic Crystal Laser for Ultra-Sensitive Biomolecule Detection

Jiacheng Sun, Tao Wang, Zeinab Jafari, Fei Gao, Xiao Lin, Hongsheng Chen, Gaofeng Wang, and Israel De Leon

***Abstract*—Plasmonic lasers provide a paradigm-changing approach for the generation of coherent light at the nanoscale. In addition to the usual properties of coherent radiation, the emission of plasmonic lasers can feature high sensitivity to the surrounding environment, which makes this technology attractive for developing high-performance and highly-integrated sensing devices. Here, we investigate a plasmonic laser architecture based on a high-Q plasmonic crystal consisting of a periodic arrangement of nanoholes on a thin gold film cladded with an organic-dye-doped glass layer as the gain material. We report an extensive full-wave numerical analysis of the device's lasing performance and its application as a biochemical sensor, showing that the proposed design features excellent figures of merit for surface sensing that in principle can be over an order of magnitude larger than those of previously reported high-performance plasmonic biosensor architectures.**

***Index Terms*—Active sensor, biomolecule detection, bulk sensing, photonic crystal, plamonic laser, surface sensing.**

Manuscript received September 30, 2020; revised January 7, 2021; accepted January 8, 2021. The work of Tao Wang was supported in part by the National Natural Science Foundation of China under Grant 61804036 and in part by Zhejiang Province Commonweal Project under Grant LGJ20A040001. The work of Zeinab Jafari and Israel De Leon was supported in part by CONACyT under Grant CN-17-109 and in part by the Federico Baur Endowed Chair in Nanotechnology. The work of Fei Gao was supported in part by National Natural Science Foundation of China under Grant 61801426 and in part by Zhejiang Provincial Natural Science Foundation (Z20F010018). The work of Gaofeng Wang was supported in part by National Key R&D Program Grant under Grant 2018YFE0120000 and in part by Zhejiang Provincial Key Research and Development Project Grant under Grant 2019C04003. *(Corresponding author: Tao Wang; Israel De Leon.)*

Jiacheng Sun is with the Engineering Research Center of Smart Microsensors and Microsystems of MOE, Hangzhou Dianzi University, and also with the School of Zhuoyue Honors, Hangzhou Dianzi University, Hangzhou 310018, China (e-mail: 17061423@hdu.edu.cn).

Tao Wang and Gaofeng Wang are with the Engineering Research Center of Smart Microsensors and Microsystems of MOE, Hangzhou Dianzi University, and also with the School of Electronics and Information, Hangzhou Dianzi University, Hangzhou 310018, China (e-mail: wangtao@hdu.edu.cn; gaofeng@hdu.edu.cn).

Zeinab Jafari and Israel De Leon are with the School of Engineering and Sciences, Tecnológico de Monterrey, Monterrey, Nuevo León 64849, Mexico (e-mail: Zjafari@tec.mx; ideleon@tec.mx).

Fei Gao, Xiao Lin, and Hongsheng Chen are with the Interdisciplinary Center for Quantum Information, College of Information Science and Electronic Engineering, Zhejiang University, Hangzhou 310027, China (e-mail: gaofeizju@zju.edu.cn; xiaolinbnwj@gmail.com; hansomchen@zju.edu.cn).

This article has supplementary material provided by the authors and color versions of one or more figures available at https://doi.org/10.1109/JSTQE.2021.3051493.

Digital Object Identifier 10.1109/JSTQE.2021.3051493

I. Introduction

SURFACE plasmons are optical surface waves formed by the coupling of an optical field to free electrons at the surface of a metal [1]. There exists two types of surface plasmon waves, i.e., surface plasmon polaritons (SPPs) and localized surface plasmons (LSPs). The former type refers to surface plasmon waves that propagate along open metallic surfaces, while the latter refers to standing waves confined to nanoscopic metallic structures. Their tight field confinement to the metal's surface [2], [3] enables these surface waves to probe minuscule fluctuations of the refractive index in the vicinity of the metal surface [4]–[6]. As such, surface plasmons have been extensively exploited for sensing applications. In particular, plasmonic biosensor technology has been widely used for biochemical applications because it offers high sensitivity, as well as capacity of real-time, label-free quantitative analysis on a broad variety of analytes, ranging from chemicals, through proteins and nucleic acids, to bacterial and viral pathogens [4], [6]–[10]. Numerous plasmonic biosensor architectures have been proposed and implemented throughout the years. Perhaps the most popular one is the surface plasmon resonance (SPR) architecture, a mature technology that makes use of the SPP supported by a thin metallic film [7]. Other more sophisticated architectures with chip-integration capacity include the use of SPPs in various waveguide configurations [11]–[14] and LSPs supported by metallic nanoparticles or nanoholes in metallic films [5], [8]. In addition, integration of plasmonic nanoparticles or nanofilms with optical fibers has also resulted in miniaturization and huge sensitivities compared to SPR architecture [15], [16]. Although a large sensitivity is appealing, the figure of merit (FOM) which is proportional to the quality factor (Q factor) of the resonance defines the ultimate sensing performance. Due to this fact, grating-like structures consisting of periodic arrays of plasmonic nanoparticles or nanoholes, typically known as plasmonic lattices or plasmonic crystals have recently attracted considerable attention as sensing platforms because they can support delocalized resonances with large Q factors and sensing FOM [17]–[20]. Indeed, the advances in plasmonic biosensor technology thus far represent a remarkable progress. Yet, improving the sensitivity and FOM of plasmonic biosensors is still of great importance as it would expand their scope of applications, for instance, achieving real-time, label-free single molecule detection, highly-integrated point of need systems, and robust clinical diagnosis [21]–[24].

Referring specifically to the sensor's transducer, the performance of all previously mentioned sensing architectures is ultimately limited by the optical losses of the system, which reduces the resonance's Q factor, thus limiting the interaction with the analyte [25] and degrading the device's FOM. Hence, a compelling approach to improve the sensing performance is to mitigate the plasmonic losses by incorporating optical gain in the system. Indeed, surface plasmon amplifiers and lasers have been demonstrated in the laboratory [26]–[28] and their prospects for applications are vast [29]. In particular, recent theoretical and experimental investigations have indicated that active plasmonic biosensing architectures can offer a significant improvement on the sensing performance [30]–[33]. While these pioneering investigations have reported an improved FOM over previously reported passive devices, more efforts are still required to demonstrate an active biosensor that satisfy key factors required for ultra-sensitive biomolecule detection, in particular the possibility of achieving a large FOM for surface sensing using a platform capable of operating at room temperature.

In this work, we investigate the sensing performance of an active plasmonic biosensor configuration based on a high-Q plasmonic crystal incorporating an organic gain medium. The structure consists of a thin gold film decorated with a two-dimensional periodic array of nanoholes and cladded with an optically-pumped Rhodamine 640-doped glass layer. The high-Q plasmonic Bloch mode supported by the passive structure favors plasmonic lasing with gain levels similar to those previously demonstrated in organic media at room temperature [34], [35]. We characterize the optical properties and sensing performance of the proposed structure through extensive finite-difference time-domain (FDTD) simulations incorporating the rate equations governing the time-domain dynamics of the gain medium's atomic populations. Our analysis indicates that lasing with a narrow linewidth of 0.24 nm is possible under practical conditions. Using wavelength interrogation, we show that such a narrow linewidth together with a large sensitivity result in FOM for bulk sensing as large as $\sim$1000 RIU^{-1} and a FOM for surface sensing of $\sim$65 RIU^{-1} for thin biolayers of the order of 5 nm. The bulk FOM, in this work, is superior to those experimentally reported in previous passive and active works based on wavelength interrogation [8], [31], [36], and comparable to values predicted recently for plasmonic-laser-based systems [32], [33]. The surface FOM is also at least one order of magnitude larger than that of passive plasmonic biosensors [37], [38], indicating that this sensing architecture has potential for ultra-sensitive biomolecule detection.

II. Principle of Operation and Structure Analysis

The optical properties of passive plasmonic crystals consisting of thin metallic films patterned with a two-dimensional array of holes have been studied extensively in the past both from the fundamental point of view [18], [39] and for biosensor applications [20], [40], [41]. In this section, we describe both the passive and active optical properties of the proposed plasmonic crystal structure.

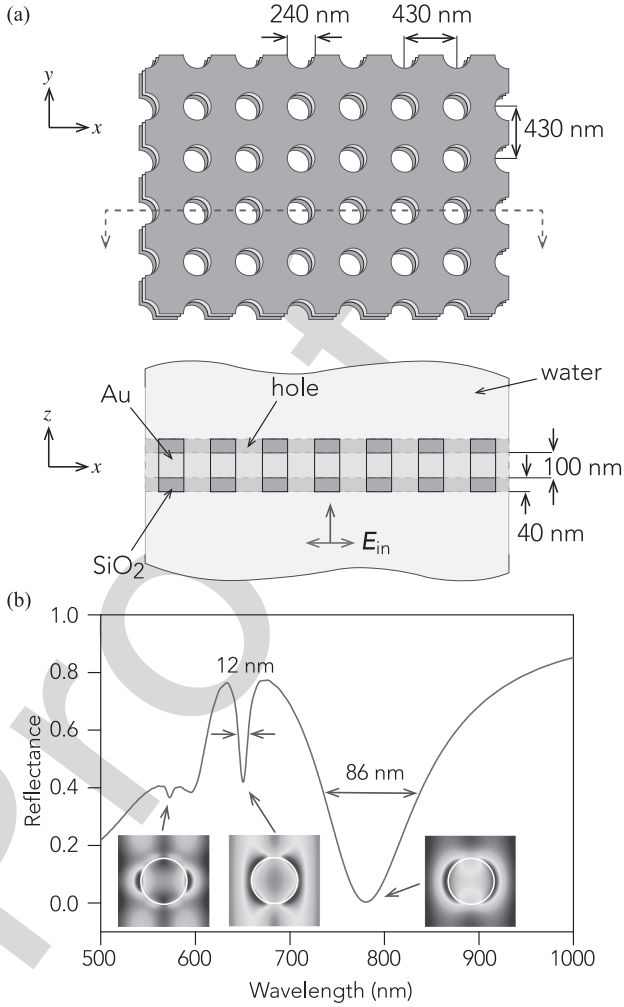

Fig. 1. Optical response of the passive structure: (a) Schematic illustration of the passive plasmonic crystal; the top panel shows a top view [(x, y)-plane] and the bottom panel shows a side view [(x, z)-plane] which is a cut along the red dashed line shown in the top panel. The medium surrounding the structure and filling the holes is water. (b) Reflection spectrum for visible and near infra-red wavelength. The broad dip corresponds to the LSP resonance of the individual nanohole, while the other two narrow dips (at 648 nm and 575 nm) are plasmonic Bloch modes of the structure. The insets illustrate the field intensity associated with the indicated spectral dips, obtained 30 nm away from the gold surface.

1) Passive Structure: We consider first the passive structure illustrated in Fig. 1(a). It consists of a gold film cladded on both sides by a thin silicon dioxide (SiO_2) layer patterned with a two-dimensional array of circular holes arranged as a squared lattice. The medium surrounding the structure and filling the holes is water. The thicknesses of the gold and each of the SiO_2 layers are 100 nm and 40 nm, respectively, the diameter of the holes is 240 nm, and the lattice period is $a = 430$ nm. We assume that the structure is illuminated by an x-polarized planewave propagating along the $+z$ direction that impinges at normal incidence onto the structure (see bottom panel of Fig. 1(a).

The optical properties of the structure are determined to a large extent by the plasmonic Bloch modes supported by the film [39]. These modes are p-polarized and can be categorized into $symmetric$ or $antisymmetric$ modes depending on whether the main magnetic field component has even or odd

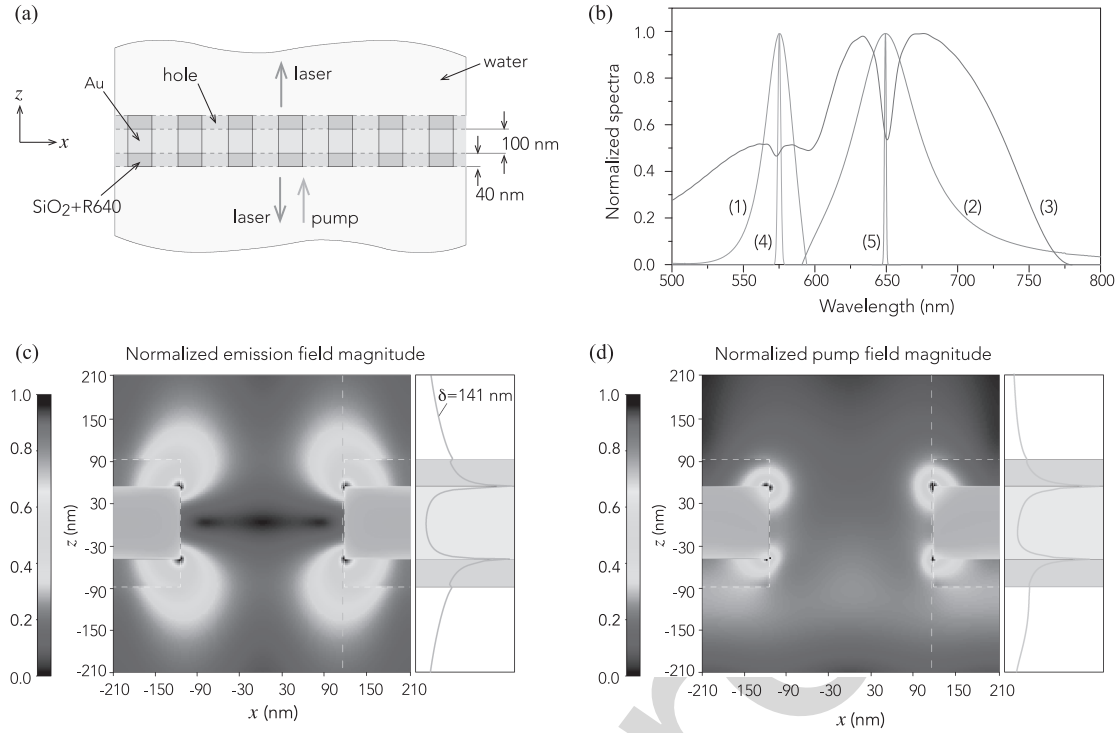

Fig. 2. Optical response of the active structure: (a) Schematic illustration of a cut through the (x, z)-plane of the active plasmonic crystal. All the parameters are the same as for the passive structure, except that the cladding is substituted by SiO_2 doped with R640 dye. (b) Relevant spectra for the active case: absorption (1) and emission (2) spectra of the R640 dye; reflection spectrum of the passive structure (3); and pump (4) and stimulated emission (5) spectra. (c) and (d) Show the normalized electric field magnitude in the (x, z)-plane through the center of the hole for the stimulated emission and pump fields, respectively. The dashed boxes superimposed indicate the location of the gain media. The curves on the right of (c,d) represent the field distribution evaluated at the points given by the dashed lines. The field in water in (c) decays exponentially with a decay constant $\delta = 141$ nm.

symmetry with respect to the $z = 0$ plane, respectively. The in-plane wavevector of these Bloch modes can be approximated by $\mathbf{k}_{\ell,m} = \mathbf{k}_{\rm SP} + \mathbf{G}$, where $\mathbf{k}_{\rm SP}$ is the wavevector of the SPP supported by the structure in the absence of the holes and $\mathbf{G} = \ell\mathbf{g}_x + m\mathbf{g}_y$ is the reciprocal lattice vector of the crystal, with $\mathbf{g}_x = \mathbf{g}_y = 2\pi/a$ being the primitive reciprocal vectors associated with the x and y directions, and ℓ and m are integers. For normal incidence illumination, only those modes with $\mathbf{k}_{\ell,m} = 0$ can be excited due to the in-plane momentum conservation, resulting in the excitation of standing-waves formed by Bloch modes with equal wavevector magnitude but opposite directions – i.e., modes associated with the indices $[\pm\ell, \pm m]$.

With this in mind, one can identify the signature of these Bloch modes in the reflectance spectrum shown in Fig. 1(b), obtained through FDTD calculations. The broad resonance, centered at the wavelength $\lambda = 778$ nm, corresponds to the symmetric $[\ell, m] = [\pm 1, 0]$ mode, while the other two narrow features centered at 648 nm and 575 nm correspond to the antisymmetric $[\pm 1, 0]$ and $[\pm 1, \pm 1]$ modes, respectively. We note that the antisymmetric $[\pm 1, 0]$ mode features a narrow linewidth of only $\sim$12 nm (corresponding to a Q factor of $\sim$54), which results from its weak coupling to radiative modes. The symmetric mode has a much broader linewidth of $\sim$86 nm. Both, symmetric and antisymmetric modes have been studied for passive sensing applications, showing similar bulk sensitivities [20]. In our case we focus on the antisymmetric $[\pm 1, 0]$ mode because its small radiative loss facilitates lasing using an optically pumped organic dye, which is attractive for its low cost and ease of fabrication.

2) Active Structure: A side view of the active structure is shown in Fig. 2(a). In this case, we have replaced the SiO_2 claddings with SiO_2 doped with Rhodamine 640 (R640) molecules, while keeping all the other structural parameters identical as those for the passive case. To model the active structure, we used an FDTD solver incorporating a semi-classical treatment for the gain medium. The semi-classical model is based on the solution of the rate equations governing the time-domain dynamics of the molecular populations in the organic gain medium [42]. The gain medium is treated as a four-energy-level system with Lorentzian emission and absorption spectra peaking at 650 nm and 575 nm, respectively. For all our simulations we have used a molecular concentration of $N = 4.5 \times 10^{19}\ \mathrm{cm}^{-3}$, and assumed that the dipole moment of such molecules is randomly oriented in space. The molecular parameters of R640 relevant for our calculations, including the radiative lifetime (4 ns) and and non-radiative damping coefficient ($3\times10^{14}\ s^{-1}$), were estimated from values previously reported in the literature for rhodamine molecules in SiO_2 at similar molecular concentration [43]. Detailed information about the FDTD model and R640 parameters can be found in the supplementary material.

The absorption (1) and emission (2) spectra of R640 used in the FDTD simulations, as well as the reflectance spectrum of the passive plasmonic crystal (3) are illustrated in Fig. 2(b). The

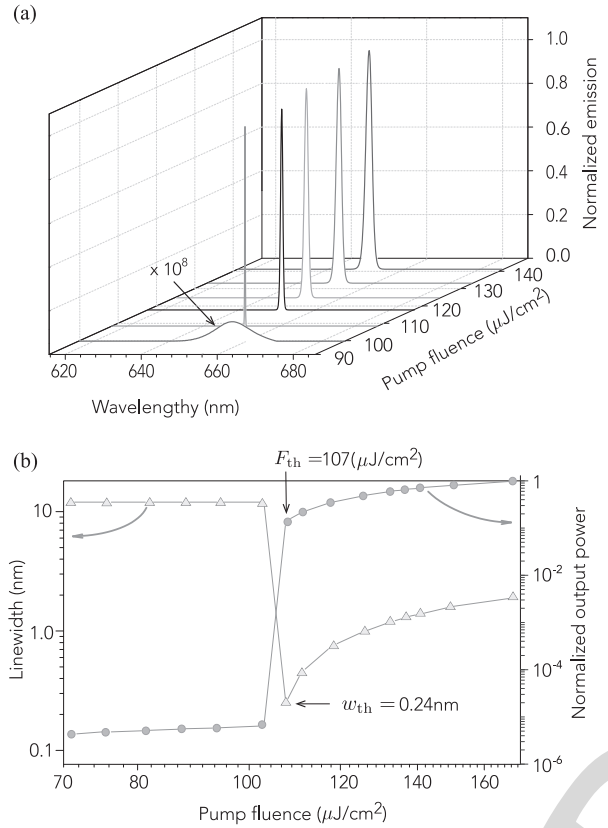

Fig. 3. Emission characteristics of the active structure: (a) Evolution of the emission spectrum as a function of the pump fluence. (b) Normalized peak value (blue circles) and spectral linewidth (orange triangles) of the emission spectrum as a function of the pump fluence. The pump threshold for laser emission is estimated as $F_{\rm th} = 107\ \mu$J/cm^2.

passive structure was optimized to support the antisymmetric $[\pm1, 0]$ and $[\pm1, \pm1]$ modes close to the peak of the emission and absorption spectra of R640, respectively, in order to facilitate the interaction of these two modes with gain medium. We have used a 200 fs pump pulse with center wavelength of $\lambda_p = 575$ nm impinging at normal incidence (see Fig. 2(a), thus exciting the $[\pm1, \pm1]$ Bloch mode of the structure. As shown in Figs. 2(c) and 2(d), this approach allows us to concentrate the pump field tightly to both surfaces of the metal film, and obtain good overlap between the pump field (the $[\pm1, \pm1]$ mode), the emission field (the $[\pm1, 0]$ mode), and the gain medium, which is crucial to achieve lasing.

The emission spectrum of the antisymmetric $[\pm1, 0]$ mode in the presence of the gain medium is calculated for a pump fluence, F, varying from 70 to 170 μJ/cm^2. The results, given in Fig. 3(a), show a broad emission spectrum characteristic of spontaneous emission for low pump fluences, and a sudden increase in the emission intensity and reduction of the spectral linewidth at $F_{\rm th} = 107\ \mu$ J/cm^2, indicating the threshold for lasing [34], [44]. The wavelength of the laser emission at the pump threshold occurs at $\lambda_e = 649.35$ nm, which is slightly shifted from the central wavelength of the antisymmetric $[\pm1, 0]$ resonance [see spectrum (1) in Fig. 2(b)]. The linewidth and normalized peak of the emission spectrum is illustrated in Fig. 3(b) as a function of F. Remarkably, the linewidth at the threshold condition is only $w_{\rm th} = 0.24$ nm and it gradually increases for larger F values. This characteristic behavior of the spectral linewidth has been reported in several experimental investigations on plasmonic nanolasers [30], [35], [44], [45]. Furthermore, similar linewidths have recently been reported experimentally for various configurations of plasmonic lasers [32], [33], [44]. The energy loss per unit length of the passive cavity can be obtained as $\alpha = \omega n_g/cQ$, where ω, c, and n_g are the angular frequency, speed of light in vacuum, and group index of the Bloch mode, respectively. Using the values $Q = 54$ and $n_g = 1.19$ obtained for the antisymmetric $[\pm1, 0]$ mode (see supplementary material), we obtain $\alpha = 2133$ cm^{-1} The threshold condition is reached when the gain supplied by the molecular medium is capable to compensate completely the loss of the cavity. However, it is important to point out that experimental investigations related to both, dielectric microlasers [46], [47] and plasmonic lasers [34], [35], have reported an enhancement in the stimulated emission rate resulting from the Purcell effect, whereby the gain provided by the molecular medium is enhanced by a factor equal to the Purcell factor of the cavity [46]. As this effect is not completely taken into account in our simulations, and our structure exhibits an averaged Purcell factor of ~ 2.1 over the gain medium (see supplementary material), we expect that the molecular concentration and pump requirements predicted by our simulations are overestimated.

III. Sensing Performance

The performance of optical biosensors are typically evaluated based on the bulk sensitivity, ($S_{\rm B}$) and surface sensitivity ($S_{\rm S}$) parameters, and their respective FOMs [8]. In particular, the $S_{\rm B}$ parameter is useful to compare the performance of different biosensor configurations, while the $S_{\rm S}$ parameter gives a more precise estimate of plasmonic affinity biosensors [48]. In what follows, we discuss the performance of the proposed active structure for both, bulk and surface sensing, assuming a constant pump fluence equal to the threshold pump fluence, $F_{\rm th}$.

We focus first on the bulk sensing performance. For spectral interrogation, the bulk sensitivity is given by $S_{\rm B} = \Delta\lambda/\Delta n_{\rm B}$, where $\Delta\lambda$ is the spectral shift of the sensing signal (the peak lasing wavelength) and $n_{\rm B}$ is the refractive index of the bulk analyte solution, which is close to the refractive index of water ($\sim$1.33). Thus, to obtain the value of $S_{\rm B}$, we assume that the refractive index of the medium around the biosensing structure is in the range $1.33 < n_{\rm B} < 1.336$. Figs. 4 a and 4(b) show FDTD calculations of the emission spectrum and peak emission wavelength as a function of $n_{\rm B}$ at the threshold pump fluence, $F_{\rm th}$. We observe a linear shift in the peak emission wavelength and no detectable change in the spectrum's linewidth. Thus, the bulk sensitivity is $S_{\rm B} = 240$ nm/RIU, obtained as the slope of the curve in Figs. 4(b), which yields a figure of merit of FOM$_{\rm B} = S_{\rm B}/w_{\rm th} = 1000$ RIU^{-1} at the lasing threshold condition.

The values of $S_{\rm B}$ and FOM$_{\rm B}$ as a function of the pump fluence are shown in Fig. 4 c. Interestingly, we note that the $S_{\rm B}$ is slightly larger below the lasing threshold. This is the result of a modest reduction in the electric field's decay constant at the lasing onset [49]. Despite this fact, the FOM$_{\rm B}$ is quite

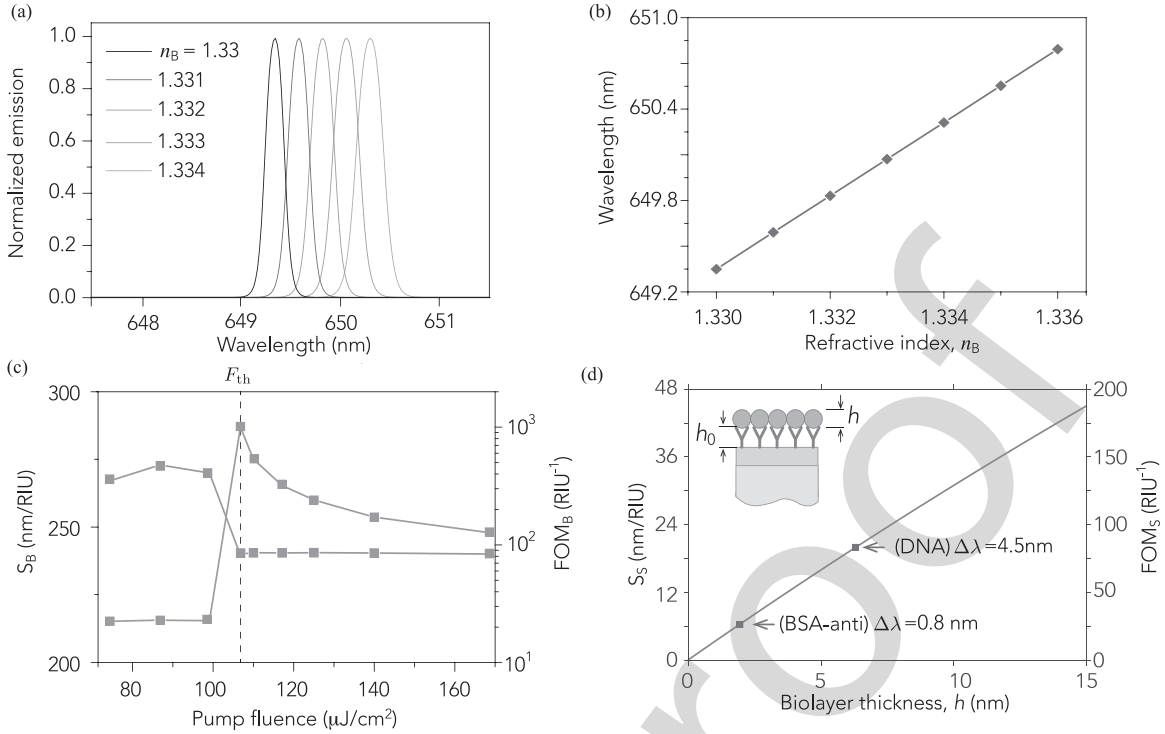

Fig. 4. Sensing performance of the active structure: (a) Spectral shift of laser emission as a function of the analyte's bulk refractive index, n_{B}. (b) Wavelength of emission peak as a function of n_{B}. (c) Bulk sensitivity (S_{B}, orange curve) and bulk sensing figure of merit ($\mathrm{FOM_B}$, blue curve) as a function of the pump fluence. The vertical dashed line indicate the threshold condition. (d) Surface sensitivity, S_{S}, and surface sensing figure of merit, $\mathrm{FOM_S}$, as a function of the biolayer thickness, h, for $h_0 = 2.5$ nm and $w = w_{\mathrm{th}}$.

small below threshold due to the large spectral linewidth. On the other hand, the $\mathrm{FOM_B}$ peaks at the threshold condition and monotonically drops as the pump fluence increases because of the increasing spectral linewidth(see Fig. 3(b). The $\mathrm{FOM_B}$ value obtained at the lasing threshold is significantly larger than that of high-performance passive plasmonic biosensors [7], [8] and experimentally demonstrated room-temperature active plasmonic sensors using spectral interrogation [31], [36].

Now, we focus on the surface sensing performance. The surface sensitivity is described by $S_{\mathrm{S}} = \Delta\lambda/\Delta n_{\mathrm{S}}$, where n_{S} is the refractive index change induced by an analyte biolayer of thickness h located at a distance h_0 from the biosensor's surface. Furthermore, it is well established that this figure can be expressed as [8]

$$S_{\mathrm{S}} = S_{\mathrm{B}} \exp(-2h_0/\delta)\left[1 - \exp(-2\,h/\delta)\right], \qquad (1)$$

where δ is the decay constant of the field into the analyte solution. The corresponding figure of merit is therefore $\mathrm{FOM_S} = S_{\mathrm{S}}/w$. For definitiveness, we consider a value of $h_0 = 2.5$ nm corresponding to the monolayer thickness of a typical bioreceptor proteins, such as A/G protein or bovine serum albumin (BSA) [50]. The values obtained for S_{S} using Eq. (1) at the lasing threshold condition are shown in Fig. 4 d. For this, we have used $w = w_{\mathrm{th}} = 0.24$ nm and $\delta = 142.8$ nm, which corresponds to the decay constant averaged over the surface of the structure (see supplementary material). Note that despite the relatively large decay constant δ, the value of S_{S} can be as large as 40 nm/RIU within the first 15 nm above the bioreceptor layer. From these results, we can estimate the wavelength shift induced by the analyte biolayer as $\Delta\lambda = S_{\mathrm{S}}\Delta n_{\mathrm{S}}$, with $\Delta n_{\mathrm{S}} = 0.24$ being the refractive index difference between water and a densely packed protein biolayer [51]. Thus, considering for instance a monolayer of BSA antibody (BSA-anti), whose thickness is $h \approx 1$ nm, we obtain $\Delta\lambda \approx 0.8$ nm. Similarly, a monolayer of a larger molecule such as DNA ($h \approx 6$ nm [52]), would results in $\Delta\lambda \approx 4.5$ nm. Clearly, the predicted spectral shifts are significantly larger than the spectral linewidth, indicating the possibility of sensing minuscule changes at the surface provided that the spectral properties of the laser remain stable. The large values of $\Delta\lambda$ compared to w_{th} reflect the large $\mathrm{FOM_S}$ of the biosensor (right scale on Fig. 4(d), which can reach a value of 125 RIU^{-1} for biolayers with a thickness in the order of 10 nm. This is contrary to the behavior observed in a passive plasmonic biosensor [49], [53] because both, S_{S} and w, are inversely proportional to δ. Thus, while a small δ certainly results in a larger S_{S} in a passive plasmonic biosensor, it does not necessary increases its $\mathrm{FOM_S}$. On the other hand, the $\mathrm{FOM_S}$ can be greatly increased in the active configuration because the narrow linewidth w is dictated by the pump fluence (Figs. 3(b) and 4(a) and is not influenced by the value of δ. For comparison, we have estimated the $\mathrm{FOM_S}$ values of typical passive plasmonic biosensors. By inserting previously reported values for plasmonic sensors, operating in a wavelength range similar to that used in this work, [38] into Eq. (1), and assuming $h = 10$ nm, $\mathrm{FOM_S}$ of 2.2 and 3.6 RIU^{-1} was obtained for LSPR and SPR sensors, respectively. Also, a $\mathrm{FOM_S}$ of 10 RIU^{-1} for $h = 10$ nm was achieved in a structure based on lattice-plasmon resonance [37]. Based on this observation we can anticipate that

the active design studied here can offer an excellent surface sensing performance.

IV. Summary and Conclusion

In conclusion, we have investigated the sensing performance of an active biosensor based on a plasmonic crystal structure incorporating an organic gain medium. The plasmonic crystal supports a high-Q Bloch mode that favors plasmonic lasing with gain levels practically attainable by organic gain media at room temperature. The optical properties, and the bulk and surface sensing performance are investigated through extensive FDTD simulations incorporating the rate equations governing the atomic population dynamics of the gain medium. Our analysis indicates that lasing with a narrow linewidth of 0.24 nm is possible under practical optical pumping conditions. We showed that the narrow laser linewidth together with a large sensitivity result in FOM for bulk sensing as large as $\sim$1000 RIU^{-1}, which is at least an order of magnitude larger than that of high-performance passive plasmonic biosensors previously reported. We also show that FOM for surface sensing can be extremely large, reaching values of $\sim$65 RIU^{-1} for thin biolayers in the order of 5 nm. We emphasize that a large surface sensing FOM is possible despite a relatively weak field confinement because, contrary to passive plasmonic sensors, the linewidth of the sensing signal is to a large extent independent of the plasmonic field confinement. The outstanding FOM values for bulk and surface sensing predicted here indicate that a high-Q active sensing architectures, such as the one studied here, have potential for low-concentration biomolecule detection.

Acknowledgment

J. Sun and T. Wang are grateful to Prof. Renmin Ma for discussion.

References

[1] S. A. Maier, *Plasmonics: Fundamentals and Applications*. New York, NY, USA: Springer, 2007.
[2] W. L. Barnes, A. Dereux, and T. W. Ebbesen, "Surface plasmon subwavelength optics," *Nature*, vol. 424, no. 6950, pp. 824–830, Aug. 2003.
[3] J. A. Schuller *et al.*, "Plasmonics for extreme light concentration and manipulation," *Nat. Mater.*, vol. 9, pp. 193–204, 2010.
[4] S. Lal, S. Link, and N. J. Halas, "Nano-optics from sensing to waveguiding," *Nat. Photon.*, vol. 1, no. 11, pp. 641–648, Nov. 2007.
[5] J. N. Anker, W. P. Hall, O. Lyandres, N. C. Shah, J. Zhao, and R. P. Van Duyne, "Biosensing with plasmonic nanosensors," *Nat. Mater.*, vol. 7, pp. 442–453, 2008.
[6] A. G. Brolo, "Plasmonics for future biosensors," *Nat. Photon.*, vol. 6, no. 11, pp. 709–713, Nov. 2012.
[7] J. Homola, Ed., *Surface Plasmon Resonance Based Sensors, Ser. Springer Ser. Chem. Sensors Biosensors*, vol. 4, Berlin, Heidelberg: Springer Berlin Heidelberg, 2006. [Onine]. Available: https://link.springer.com/book/10.1007/b100321
[8] B. pakov, P. Wrobel, M. Bockova, and J. Homola, "Optical biosensors based on plasmonic nanostructures: A review," *Proc. IEEE Proc. IRE*, vol. 104, no. 12, pp. 2380–2408, Dec. 2016.
[9] A. B. Dahlin, N. J. Wittenberg, F. Hk, and S.-H. Oh, "Promises and challenges of nanoplasmonic devices for refractometric biosensing," *Nanophotonics*, vol. 2, no. 2, pp. 83–101, 2013.
[10] J. A. Jackman, A. Rahim Ferhan, and N.-J. Cho, "Nanoplasmonic sensors for biointerfacial science," *Chem. Soc. Rev.*, vol. 46, no. 12, pp. 3615–3660, 2017.
[11] J. Dostalek *et al.*, "Surface plasmon resonance biosensor based on integrated optical waveguide," *Sensors Actuators, B: Chem.*, vol. 76, pp. 8–12, 2001.
[12] O. Krupin, H. Asiri, C. Wang, R. N. Tait, and P. Berini, "Biosensing using straight long-range surface plasmon waveguides," *Opt. Exp.*, vol. 21, no. 1, p. 698, Jan. 2013.
[13] W. R. Wong, F. R. M. Adikan, and P. Berini, "Long-range surface plasmon y-junctions for referenced biosensing," *Opt. Exp.*, vol. 23, no. 24, Nov. 2015, Art. no. 31098.
[14] Y. Gao, Q. Gan, Z. Xin, X. Cheng, and F. J. Bartoli, "Plasmonic mach-zehnder interferometer for ultrasensitive on-chip biosensing," *Amer. Chem. Soc. Nano*, vol. 5, pp. 9836–9844, 2011.
[15] H. Han *et al.*, "A large detection-range plasmonic sensor based on an h-shaped photonic crystal fiber," *Sensors*, vol. 20, no. 4, 2020, Art. no. 1009.
[16] Y. Esfahani Monfared, "Overview of recent advances in the design of plasmonic fiber-optic biosensors," *Biosensors*, vol. 10, no. 7, 2020, Art. no. 77.
[17] F. J. Garca de Abajo, "Colloquium : Light scattering by particle and hole arrays," *Rev. Modern Phys.*, vol. 79, no. 4, pp. 1267–1290, Oct. 2007.
[18] F. J. Garcia-Vidal, L. Martin-Moreno, T. W. Ebbesen, and L. Kuipers, "Light passing through subwavelength apertures," *Rev. Modern Phys.*, vol. 82, no. 1, pp. 729–787, Mar. 2010.
[19] V. G. Kravets, A. V. Kabashin, W. L. Barnes, and A. N. Grigorenko, "Plasmonic surface lattice resonances: A review of properties and applications," *Chemincal Rev.*, vol. 118, pp. 5912–5951, 2018.
[20] M. Vala, C. T. Ertsgaard, N. J. Wittenberg, and S.-H. Oh, "Plasmonic sensing on symmetric nanohole arrays supporting high-q hybrid modes and reflection geometry," *Amer. Chem. Soc. Sensors*, vol. 4, no. 12, pp. 3265–3274, Dec. 2019.
[21] P. Zijlstra, P. M. Paulo, and M. Orrit, "Optical detection of single non-absorbing molecules using the surface plasmon resonance of a gold nanorod," *Nat. Nanotechnol.*, vol. 7, pp. 379–382, 2012.
[22] S. Chen, Mikael Svedendahl, R. P. Van Duyne, and K. Mikael, "Plasmon-enhanced colorimetric elisa with single molecule sensitivity," *Nano Lett.*, vol. 11, pp. 1826–1830, 2011.
[23] J. Liu, M. Jalali, S. Mahshid, and S. Wachsmann-Hogiu, "Are plasmonic optical biosensors ready for use in point-of-need applications?" *Analyst*, vol. 45, pp. 364–384, 2020.
[24] E. Mauriz, P. Dey, and L. M. Lechuga, "Advances in nanoplasmonic biosensors for clinical applications," *Analyst*, vol. 144, pp. 7105–7129, 2019.
[25] B. Dastmalchi, P. Tassin, T. Koschny, and C. M. Soukoulis, "A new perspective on plasmonics: Confinement and propagation length of surface plasmons for different materials and geometries," *Adv. Opt. Mater.*, vol. 4, pp. 177–184, 2016.
[26] P. Berini and I. De Leon, "Surface plasmon-polariton amplifiers and lasers," *Nat. Photon.*, vol. 6, pp. 16–24, 2012.
[27] Z. Wang, X. Meng, A. V. Kildishev, A. Boltasseva, and V. M. Shalaev, "Nanolasers enabled by metallic nanoparticles: From spasers to random lasers," *Laser Photon. Rev.*, vol. 11, pp. 1–15, 2017.
[28] H. Wu *et al.*, "Plasmonic nanolasers: Pursuing extreme lasing conditions on nanoscale," *Adv. Opt. Mater.*, vol. 7, pp. 1–16, 2019.
[29] R.-M. Ma and R. F. Oulton, "Applications of nanolasers," *Nat. Nanotechnol.*, vol. 14, pp. 12–22, 2019.
[30] R.-M. Ma, S. Ota, Y. Li, S. Yang, and X. Zhang, "Explosives detection in a lasing plasmon nanocavity," *Nat. Nanotechnol.*, vol. 9, no. 8, pp. 600–604, Aug. 2014.
[31] S. Wang *et al.*, "High-yield plasmonic nanolasers with superior stability for sensing in aqueous solution," *ACS Photon.*, vol. 4, no. 6, pp. 1355–1360, Jun. 2017.
[32] W. Zhu *et al.*, "Surface plasmon polariton laser based on a metallic trench fabry-perot resonator," *Sci. Adv.*, vol. 3, no. 10, Oct. 2017, Art. no. e1700909.
[33] P.-J. Cheng *et al.*, "High-performance plasmonic nanolasers with a nanotrench defect cavity for sensing applications," *ACS Photon.*, vol. 5, no. 7, pp. 2638–2644, Jul. 2018.
[34] J. Y. Suh *et al.*, "Plasmonic bowtie nanolaser arrays," *Nano Lett.*, vol. 12, no. 11, pp. 5769–5774, Nov. 2012.
[35] A. Yang *et al.*, "Real-time tunable lasing from plasmonic nanocavity arrays," *Nat. Commun.*, vol. 6, no. 1, Nov. 2015, Art. no. 6939.
[36] X.-Y. Wang *et al.*, "Lasing enhanced surface plasmon resonance sensing," *Nanophotonics*, vol. 6, no. 2, pp. 472–478, Mar. 2017.
[37] B. pakov and J. Homola, "Sensing properties of lattice resonances of 2D metal nanoparticle arrays: An analytical model," *Opt. Exp.*, vol. 21, 2013, Art. no. 27490.

[38] B. pakov, M. L. Ermini, and J. Homola, "High-performance biosensor exploiting a light guidance in sparse arrays of metal nanoparticles," *Opt. Lett.*, vol. 44, no. 7, pp. 1568–1571, 2019.
[39] W. Dickson, G. A. Wurtz, and A. V. Zayats, Photonics: Photonics technology and instrumentation, III. Wiley, 2015, *ch. 3 - Plasmonic Crystals: Controlling Light With Periodically Structured Metal Films*, Available: https://link.springer.com/book/10.1007/b100321
[40] V. Malyarchuk *et al.*, "High performance plasmonic crystal sensor formed by soft nanoimprint lithography," *Opt. Exp.*, vol. 13, 2005, Art. no. 5669.
[41] A. De Leebeeck, K. Kumar, A. G. Brolo, R. Gordon, and D. Sinton, "On-chip detection with nanohole arrays," *Anal. Chem.*, pp. 4094–4100, 2007.
[42] S.-H. Chang and A. Taflove, "Finite-difference time-domain model of lasing action in a four-level two-electron atomic system," *Opt. Exp.*, vol. 12, 2004, Art. no. 3827.
[43] A. Lewkowicz *et al.*, "Concentration-dependent fluorescence properties of rhodamine 6 G in titanium dioxide and silicon dioxide nanolayers," *The J. Phys. Chem. C*, vol. 116, no. 22, pp. 12 304–12 311, 2012.
[44] T. K. Hakala *et al.*, "Lasing in dark and bright modes of a finite-sized plasmonic lattice," *Nat. Commun.*, vol. 8, no. 1, Apr. 2017, Art. no. 13687.
[45] H. T. Rekola, T. K. Hakala, and P. Trm, "One-dimensional plasmonic nanoparticle chain lasers," *ACS Photon.*, vol. 5, no. 5, pp. 1822–1826, May 2018.
[46] A. J. Campillo, J. D. Eversole, and H. B. Lin, "Cavity quantum electrodynamic enhancement of stimulated emission in microdroplets," *Phys. Rev. Lett.*, vol. 4, pp. 437–440, 1991.
[47] M. Djiango, T. Kobayashi, and W. J. Blau, "Cavity-enhanced stimulated emission cross section in polymer microlasers," *Appl. Phys. Lett.*, vol. 93, no. 14, Oct. 2008, Art. no. 143306.
[48] J. Li *et al.*, "Revisiting the surface sensitivity of nanoplasmonic biosensors," *Amer. Chem. Soc. Photon.*, vol. 2, pp. 425–431, 2015.
[49] F. Mazzotta *et al.*, "Influence of the evanescent field decay length on the sensitivity of plasmonic nanodisks and nanoholes," *Amer. Chem. Soc. Photon.*, vol. 2, pp. 256–262, 2015.
[50] Z. Wang, C. He, X. Gong, J. Wang, and T. Ngai, "Measuring the surface-surface interactions induced by serum proteins in a physiological environment," *Langmuir*, vol. 32, pp. 12 129–12 136, 2016.
[51] Y. Gao, Z. Xin, Q. Gan, X. Cheng, and F. J. Bartoli, "Plasmonic interferometers for label-free multiplexed sensing," *Opt. Exp.*, vol. 21, p. 5859, 2013.
[52] M. Piliarik *et al.*, "High-resolution biosensor based on localized surface plasmons," *Opt. Exp.*, vol. 20, p. 672, 2012.
[53] M. Svedendahl, S. Chen, A. Dmitriev, and M. Kll, "Refractometric sensing using propagating versus localized surface plasmons: A direct comparison," *Nano Lett.*, vol. 9, pp. 4428–4433, 2009.

Jiacheng Sun is currently studying with Hangzhou Dianzi University, Hangzhou, China. His research mainly focuses on light–matter interaction in low-dimensional structures, especially exploring novel optical properties of nanolasers.

Tao Wang received the Ph.D. degree in physics from the Université de Nice-Sophia Antipolis, Nice, France, in 2016. From 2013 to 2016, he was with the Institut Non Linéaire de Nice (now the Institut de Physique de Nice), Nice, France, as a Ph.D. Student. Since 2016, he has been a Postdoctoral Fellow with the Institut National de la Recherche Scientifique, Quebec City, QC, Canada. He is currently an Associate Professor with the School of Electronics and Information, Hangzhou Dianzi University, Hangzhou, China. His research interests include micro or nanoscale laser dynamics, optical sensors based on lasers, nonlinear optics, light–matter interactions, and optical materials.

Zeinab Jafari received the Ph.D. degree in electrical engineering from Shiraz University, Shiraz, Iran, in 2018. She is currently a Postdoctoral Fellow with Nanophotonics Research Laboratory, School of Engineering and Sciences, Tecnologico de Monterrey, Monterrey, Mexico. Her research interests include plasmonics, nanophotonics, integrated optics, and nonlinear optics.

Fei Gao received the master's degree in condensed matter physics from Nanjing University, Nanjing, China, and the Ph.D. degree in physics and applied physics from Nanyang Technological University (NTU), Singapore, in 2016. Prior to NTU, he held a research position with Biomedical Optics, the Shenzhen Institutes of Advanced Technology, Shenzhen, China. He currently holds a tenure-track position with Zhejiang University, Hangzhou, China. His current research interests include electromagnetic wave theory, topological electromagnetics, metamaterials, plasmonics, and photonic crystals.

Xiao Lin received the B.S. degree in 2011 in optical science and engineering from Zhejiang University, Hangzhou, China, where he is currently working toward the Ph.D. degree with the College of Information Science and Electronic Engineering. During the Ph.D. studies, he was a Visiting Student with the Nanyang Technological University, Singapore, and the Massachusetts Institute of Technology, Cambridge, MA, USA. His current research interests include 2-D materials, surface plasmons, and electromagnetic radiation.

Hongsheng Chen received the B.S. and Ph.D. degrees in electrical engineering from Zhejiang University, Hangzhou, China, in 2000 and 2005, respectively. In 2005, he joined as an Assistant Professor with Zhejiang University, where he was an Associate Professor in 2007 and a Full Professor in 2011. From 2006 to 2008, he was a Visiting Scientist with the Research Laboratory of Electronics, Massachusetts Institute of Technology, Cambridge, MA, USA, where he was a Visiting Professor from 2013 to 2014. His current research interests include metamaterials, invisibility cloaking, transformation optics, and theoretical and numerical methods of electromagnetics. He was the recipient of the National Excellent Doctoral Dissertation Award in China in 2008, the Zhejiang Provincial Outstanding Youth Foundation in 2008, the National Youth Top-Notch Talent Support Program in China in 2012, the New Century Excellent Talents in University of China in 2012, the National Science Foundation for Excellent Young Scholars of China in 2013, the Distinguished Chang Jiang Scholar Professorship from the Chinese Ministry of Education in 2014, and the National Science Foundation for Distinguished Young Scholars of China in 2016. He is a Regular Reviewer for many international journals on electromagnetics, physics, optics, and electrical engineering, the Topical Editor of the *Journal of Optics*, and is on the Editorial Board of Nature's *Scientific Reports* and *Progress in Electromagnetics Research*.

Gaofeng Wang received the Ph.D. degree in electrical engineering from the University of Wisconsin-Milwaukee, Milwaukee, WI, USA, in 1993, and the Ph.D. degree in scientific computing from Stanford University, Stanford, CA, USA, in 2001. From 1993 to 1996, he was a Scientist with Tanner Research, Inc., Pasadena, CA. From 1996 to 2001, he was a Principal Research and Development Engineer with Synopsys, Inc., Mountain View, CA. In 1999, he was a Consultant with Bell Laboratories, Murray Hill, NJ, USA. From 2001 to 2003, he was a Chief Technology Officer of Intpax, Inc., San Jose, CA. From 2004 to 2010, he was a Chief Technical Officer with Siargo Inc., Santa Clara, CA. From 2004 to 2013, he was a Professor and the Head with the CJ Huang Information Technology Research Institute, Wuhan University, Wuhan, China. From 2010 to 2013, he was the Chief Scientist with Lorentz Solution, Inc., Santa Clara. He is currently a Distinguished Professor with Hangzhou Dianzi University, Hangzhou, China. He has authored or coauthored more than 210 journal articles and holds 30 patents. His current research interests include integrated circuit and microelectromechanical system design and simulation, computational electromagnetics, electronic design automation, and wavelet applications in engineering.

Israel De Leon received the Ph.D. degree in electrical engineering from the University of Ottawa, Ottawa, ON, Canada, in 2011 for his theoretical and experimental work in active plasmonics. His Ph.D. dissertation was recognized with the Governor General's Gold Medal for the highest academic standing at the graduate level in Canada. He was a Postdoctoral Fellow and a Research Associate with the Max Planck Centre for Extreme and Quantum Photonics, Canada. Since 2018, he has been a Faculty Member and Leader of the Nanophotonics Research Laboratory at the School of Engineering and Sciences, Tecnologico de Monterrey, Monterrey, Mexico. Since 2019, he has also been an Adjoint Professor with the School of Engineering and Computer Sciences, University of Ottawa. His research interest include, both theoretical and experimental, plasmonics, nanophotonics, and nonlinear optics, aiming at multidisciplinary applications.